350 °C. Waveguides were patterned using DUV lithography and HBr Reactive-ion etching, then covered with 1.5 μm m thick silica. Waveguides of 475 nm width and 20 mm length were fabricated and light was coupled horizontally using lensed fibers.

On the other hand, SOI waveguides were also fabricated for comparison. These were processed from SOI wafers with 220 nm Si thickness, patterned with deep-UV lithography and covered with silica after the etching process. Their dimensions were 445×220 nm for transverse-electric (TE) polarization and 485×220 nm for transverse-magnetic (TM) polarization. Total length was 25 mm and light was coupled through grating couplers.

Figure 1 shows scanning electron microscopy (SEM) micrographs of the facets. Propagation and coupling loss were measured by characterizing waveguides of different lengths (results are shown in Table 1).

Fig. 1. SEM images of the amorphous silicon (a), TM SOI (b) and TE SOI (c). Air bubbles visible in the SOI samples were generated during facet preparation with HF to increase SEM contrast.

3. Four-wave-mixing: Re$\{\gamma\}$

Two continuous wave (cw) lasers were coupled to the waveguides, a pump beam with power $P_P(0)$ and a weaker signal beam with power $P_S(0)$, generating an idler signal at the waveguide output $P_i(L)$. We measured the conversion efficiency as a function of the wavelength separation between pump and signal by using an optical spectrum analyzer (OSA) as shown in Fig. 2. Assuming that at these power levels (below 15 dBm) TPA is negligible, we can use Eq. (1) as in Ref. [8].

$$P_i(L) = e^{-\alpha_0 L}(\eta Re\{\gamma\}P_P(0)L_{eff})^2 P_s(0) \tag{1}$$

where α_0 is the propagation loss, L the waveguide total length, and L_{eff} the effective length, defined as $[1-\exp(-\alpha_0 L)]/\alpha_0$

Finally, the conversion efficiency η is given by [9, 10]:

$$\eta^2 = \frac{\alpha_0^2}{\alpha_0^2+\Delta\beta^2}\left(1+4e^{-\alpha_0 L}\frac{sin^2(L\Delta\beta/2)}{1-e^{-\alpha_0 L}}\right) \tag{2}$$

where the phase mismatch for a detuning $\Delta\lambda = \lambda_p - \lambda_s$ is

$$\Delta\beta = \frac{2\pi c D_\lambda}{\lambda_p^2}\Delta\lambda^2 \tag{3}$$

where D_λ is the chromatic dispersion parameter. One can relate the idler output to the signal output by rearranging Eq. (1) obtaining

$$\frac{P_i(L)}{P_s(L)} = (\eta Re\{\gamma\}P_P(0)L_{eff})^2 \tag{4}$$

#171978 - $15.00 USD Received 5 Jul 2012; revised 5 Oct 2012; accepted 9 Oct 2012; published 11 Feb 2013

which is the equation used for the calculation of $Re\{\gamma\}$ and dispersion D_λ from the OSA spectra. Results are shown in Fig. 3 and parameters of the fit are shown in Table 1. The sign of the dispersion cannot be extracted from this method, but knowing the waveguide geometry, we calculated the dispersion of the waveguides using Finite Elements simulations. We found a good fit with the numeric results shown in Table 1 within a 10% error, so this gave us the sign of dispersion. Dispersion of the SOI samples was also experimentally characterized with an interferometric setup obtaining a good agreement too [11].

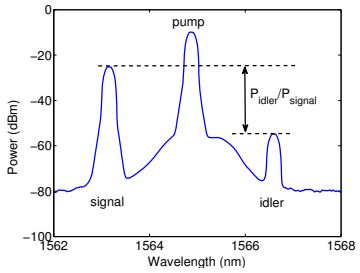

Fig. 2. With 13 dBm pump power in waveguide a signal to idler conversion efficiency of -29.5 dB was measured in the FWM experiment.

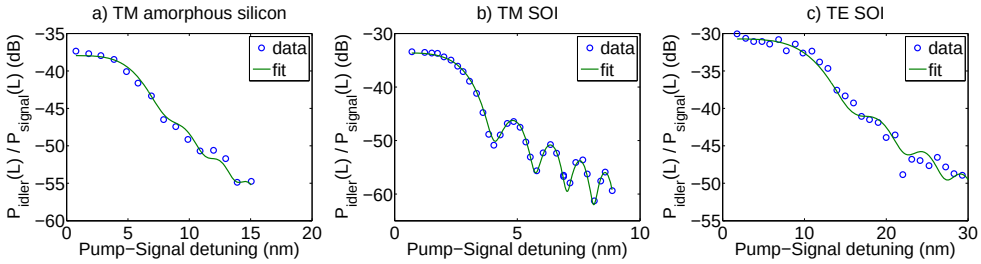

Fig. 3. Four wave mixing conversion efficiency bandwidth. Pump power: 7.5 dBm (sample a), 14 dBm (sample b), 9 dBm (sample c). Dots are experimental points and the solid line is the fit to Eq. (4).

We also show in Fig. 4 the conversion efficiency for different input pump powers, where a slope very close to 2 was observed in all cases, confirming that the parametric conversion depends quadratically on the pump power.

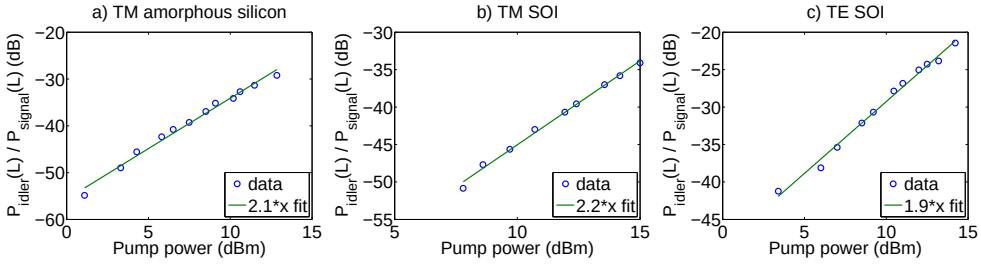

Fig. 4. Four wave conversion efficiency versus pump power. Dots: experimental points, solid line: linear fit. The slope of the linear fit in dB represents the power of the conversion efficiency versus pump power, which is close to 2 in all cases.

#171978 - $15.00 USD Received 5 Jul 2012; revised 5 Oct 2012; accepted 9 Oct 2012; published 11 Feb 2013

4. Nonlinear loss measurements: Im$\{\gamma\}$

Two-photon absorption is a well-known process in silicon waveguides. In a waveguide, we can consider it as the imaginary part of the gamma coefficient of the waveguide by using this differential equation:

$$\frac{dP}{dz} = -\alpha_0 P(z) - 2|Im(\gamma)|P(z)^2 \tag{5}$$

where P is the signal power through the waveguide, α is the linear loss of the waveguide, and $Im(\gamma)$ is the imaginary part of the γ coefficient (we use the absolute value because we want to stress its loss character in the equation with a negative sign).

The solution of the differential equation shown in Eq. (5) after a distance L is given by:

$$P(L) = \frac{e^{-\alpha_0 L}}{1+2|Im(\gamma)|L_{eff}P_0}P_0 \tag{6}$$

where P_0 is the input power in the waveguide. Therefore the ratio between the transmission at low power ($T_{LP} = e^{-\alpha_0 L}$) and the transmission at high power ($T_{HP} = P(L)/P_0$) represents only the nonlinear loss T_{NL}^{-1}:

$$T_{NL}^{-1} = \frac{T_{LP}}{T_{HP}} = 1 + 2|Im(\gamma)|L_{eff}P_0 \tag{7}$$

which is a linear function on P_0. The slope of the curve can give us the two-photon absorption coefficient of our waveguide as in [8]. However, this equation is only valid for instantaneous transmission values. When a pulsed signal is sent, and the transmission is averaged over time, the measured transmission would be the integral of the output, which we can define as:

$$\tilde{T} = \frac{\int P(t,L)dt}{\int P_0(t)dt} \tag{8}$$

where $\tilde{T}$ represent the averaged transmission of a pulsed signal with an input shape given by $P_0(t)$. With this definition, the ratio with the transmission at low power would be given by:

$$\tilde{T}_{NL}^{-1} = \frac{\tilde{T}_{LP}}{\tilde{T}_{HP}} = \frac{\int P_0(t)dt}{\int \frac{P_0(t)}{1+2|Im(\gamma)|L_{eff}P_0(t)}dt} \tag{9}$$

which depends on the actual pulse shape $P_0(t)$ that is introduced. If the pulsed signal has a rectangular shape, one can use Eq. (7), but if the shape is different, the integral in Eq. (9) must be solved, as the result differs significantly. The reason for this variation is the fact that the flanks of the pulse are not affected as hardly by TPA as the peak. Therefore, the overall energy transmission is higher than for the case of cw excitation. For the particular case of a $sech^2$ shape, which corresponds to the output of our laser, the result of Eq. (9) is given by:

$$\tilde{T}_{NL}^{-1} = \frac{\tilde{T}_{LP}}{\tilde{T}_{HP}}\bigg|_{sech^2\ shape} = \frac{\sqrt{\delta}\sqrt{\delta+1}}{\ln(\sqrt{\delta}+\sqrt{\delta+1})} \text{ where } \delta = 2|Im(\gamma)|L_{eff}P_{0peak} \tag{10}$$

We measured this parameter with a power meter using a picosecond laser at a wavelength of 1539 nm and a variable attenuator. The results are shown in Fig. 5, where the curves were fitted to Eq. (10) in order to extract the $Im(\gamma)$ parameter shown in Table 1.

#171978 - $15.00 USD Received 5 Jul 2012; revised 5 Oct 2012; accepted 9 Oct 2012; published 11 Feb 2013

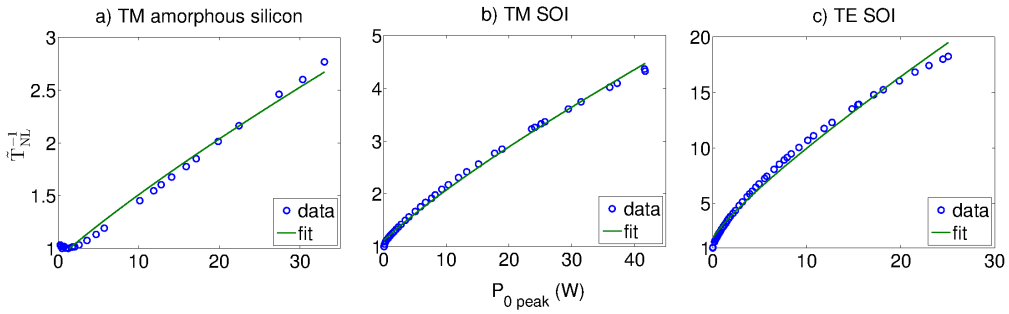

Fig. 5. Transmission versus waveguide peak power (note the difference in the y-scale among the three plots). Solid line shows the fit for $sech^2$ pulses using Eq. (10).

5. Time-resolved measurements and simulations

We characterize the samples with a time-resolved phase-sensitive technique similar to the one described in [12]. The setup is shown in Fig. 6. In this technique, we divide a 1 ps laser pulse into three pulses, one of them intense (pump) and two identical weak ones (a reference and a probe). Then we combine the pump very close to the probe, changing their separation with a variable delay line. Finally the amplitude and phase of the probe is monitored as a function this delay by using a lock–in amplifier.

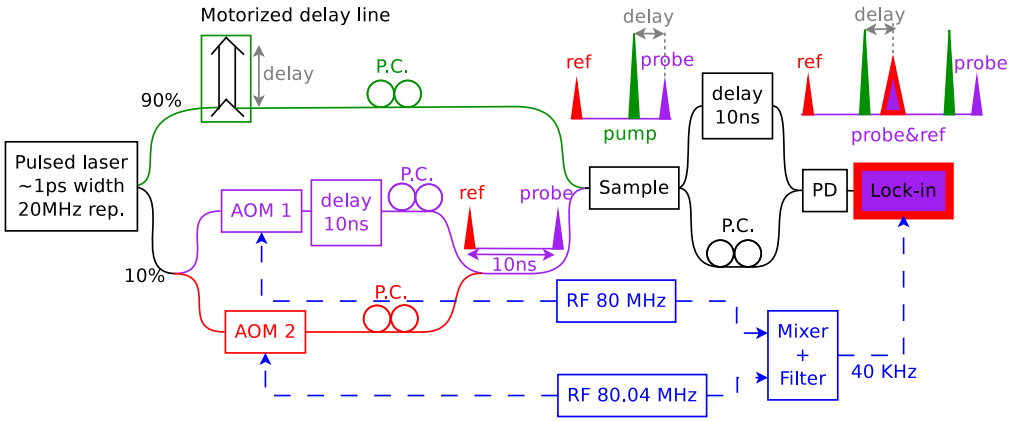

Fig. 6. Time resolved characterization setup. PD: photodiode, PC: polarization controller, AOM: acousto-optic modulator.

In Fig. 7 we observe both Kerr and carrier effect in the TM amorphous silicon compared to SOI TM and TE strip waveguides. They produce opposite phase shifts because Kerr produces an increase in refractive index ($\Delta n > 0$) and carriers decrease it ($\Delta n < 0$). The dynamics of each of these processes is also very different. During the pump pulse, an instantaneous phase change is due to Kerr effect, together with an amplitude decrease. This decrease is due to cross-absorption modulation (XAM), which consists of a two-photon absorption (TPA) process where one of the photons comes from the pump and the other one comes from the probe. Once the pump pulse is gone, in the SOI samples there is a phase response with opposite sign that remains for all the measurement range. This is due to the carrier plasma effect, also known as free-carrier dispersion (FCD).

The measurement of the amplitude attenuation due to XAM is affected by the artifact re-

#171978 - $15.00 USD Received 5 Jul 2012; revised 5 Oct 2012; accepted 9 Oct 2012; published 11 Feb 2013

ported in [8], where the abrupt phase changes create a frequency shift in the probe signal modifying the signal detected in the lock-in amplifier.

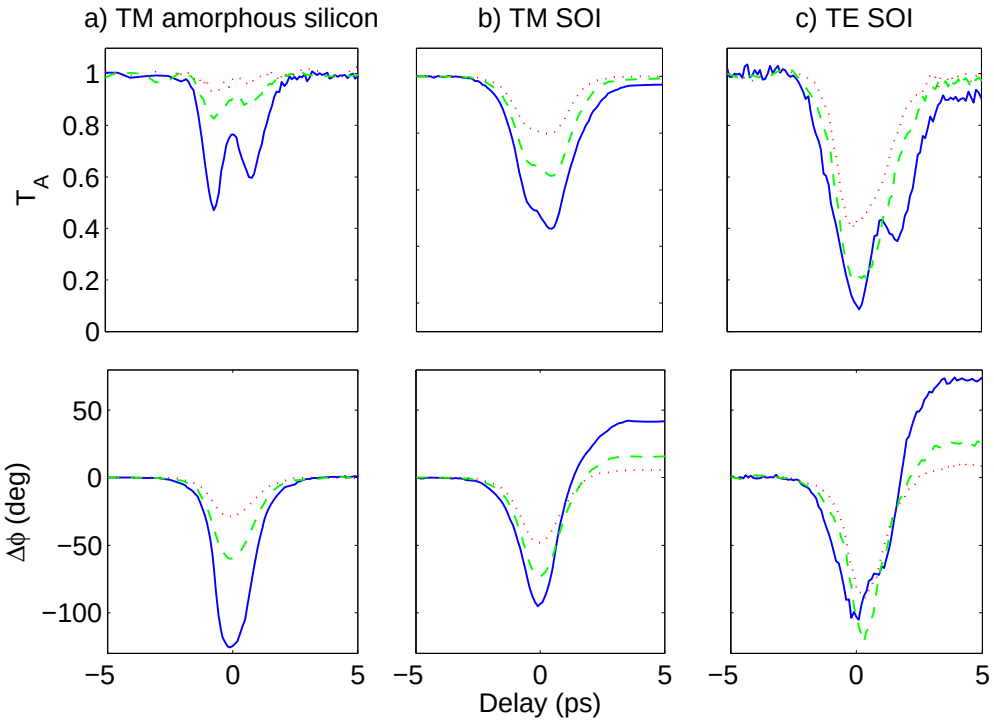

Fig. 7. Time resolved measurements for different peak powers in waveguide. (sample a) 0.8W (—), 0.4W (- -), 0.2W (· ·) (sample b) 6W (—), 3W (- -), 1.5W (· ·) (sample c) 3W (—), 1.5W (- -), 0.75W (· ·)

We used the nonlinear Schrödinger equation to simulate the propagation of pump and probe pulses in optical waveguides, neglecting the Raman term, the self-steepening term and considering dispersion up to the second order [13]. Solving the equation with the symmetrized split-step Fourier method as in [14, 15], we cross-check simulations with experimental measurements in Figure 8. The output of the simulation is the envelope of the pump, probe and reference pulses, so in order to extract the output of the lock-in amplifier we calculated the overlap integral of the probe and reference pulses:

$$|T_A|e^{j\phi} = \frac{\int E_{\text{ref}}(\tau)E^*_{\text{probe}}(\tau)\,\mathrm{d}\tau}{\int |E_{\text{ref}}(\tau)|^2\,\mathrm{d}\tau} \tag{11}$$

where T_A and ϕ are respectively the transmitted amplitude and phase measured in the lock–in amplifier.

6. Results

Table 1 shows all the numeric results of this work. First, it is worth noting that the TM SOI sample is weakly confined in the vertical direction because the thickness is 220 nm, while confinement of the TM a-Si sample was considerably better, as the thickness was 250 nm. This is the reason why both real and imaginary parts of γ are much higher for TE SOI than for the TM SOI. A similar behavior was reported in Ref. [8]. The FOM of the TM SOI (0.69) is also

#171978 - $15.00 USD Received 5 Jul 2012; revised 5 Oct 2012; accepted 9 Oct 2012; published 11 Feb 2013

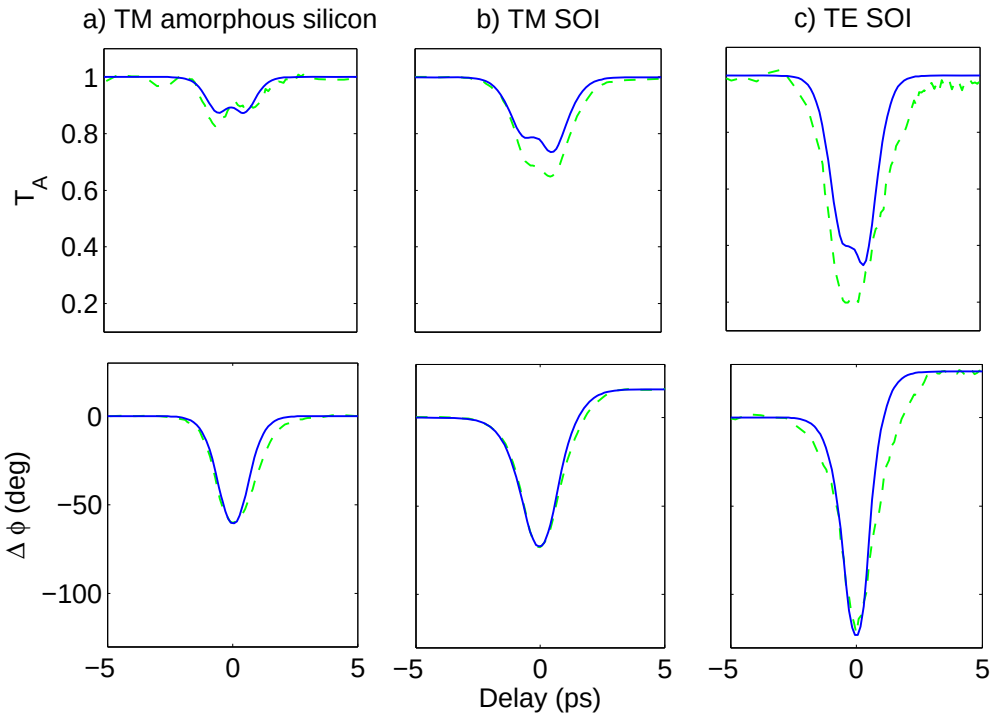

Fig. 8. Time resolved measurements (- -) and simulations (—) for 0.4W (sample a), 3W (sample b) and 1.5W (sample c) peak power in waveguide.

higher than the TE SOI (0.43) and higher than bulk silicon FOM (0.32) because there is more energy going through the silica cladding than for the TE SOI. On the other hand, the TM a-Si sample has a similar $Re\{\gamma\}$ than the TE SOI, but much lower $Im\{\gamma\}$, making the FOM several times higher. The explanation of this, as claimed in the literature [5, 7], is the fact that a-Si has a higher band-gap, which makes TPA lower while keeping a similar Kerr coefficient. The measured nonlinear coefficient n_2 in a-Si was $17.5 \cdot 10^{-5}\text{cm}^2/\text{GW}$ which is 4.6 times higher than in the TM crystalline silicon SOI sample ($3.8 \cdot 10^{-5}\text{cm}^2/\text{GW}$) while the β_{TPA} was 1.5 times lower (0.23 in the a-Si versus 0.35 cm/GW). Regarding the stability, we did not observe any degradation neither in the FWM conversion efficiency nor any change in the losses when using the pulsed laser at maximum power after one hour of operation, which means that the material is more stable than the one reported in Ref. [7], which degraded significantly after few minutes of exposure. The reason for this is probably differences in the fabrication conditions, and this is a topic under investigation but out of the scope of this work.

Time-resolved measurements show that the a-Si waveguide not only has a low TPA but also that free carriers have a negligible role. This is clear from Fig. 7 where the phase curve does not have any slow component associated to the free carrier contribution. On the contrary, the response of strip waveguides shows a long tail with $\Delta n < 0$ for delay times longer than 1 ns. This is confirmed by the FCD parameter (σ_n), defined in [14] and shown in Table 1. This feature would considerably reduce the undesired patterning effects when modulating a real bit pattern.

Finally, the FOM reported in this work is also higher than the one shown in Refs. [8, 18] which was based on a hybrid waveguide with a nonlinear organic polymer in a slot configuration, yielding a FOM of 2.19. It is worth pointing out that amorphous Si is a more suitable

#171978 - $15.00 USD Received 5 Jul 2012; revised 5 Oct 2012; accepted 9 Oct 2012; published 11 Feb 2013

Table 1. Properties of the amorphous silicon waveguide compared with 445×220 nm and 485×220 nm (TE and TM) SOI waveguides. The dispersion value was obtained through the fit of the FWM conversion bandwidth and its sign simulating the dispersion of the structure. Figure of merit is defined as in paper [16] and A_{eff} as in [17].

Sample	TM a-Si	TM SOI	TE SOI
Coupling loss (dB)	7.5	6	6
Propagation loss (dB/cm)	4	1.9	4.9
L_{eff} (mm)	9.14	15.2	8.34
D_λ (ps/(km· nm))	-6500	-19800	-1200
$-\sigma_n$ (10^{-21} cm^3)	< 1	10.7	13.8
A_{eff} (μm^2)	0.21	0.33	0.13
$Re\{\gamma\}$ (W$\cdot$m)$^{-1}$	332	47	361
$\lvert Im\{\gamma\}\rvert$ (W$\cdot$m)$^{-1}$	5.43	5.44	68.08
$FOM = \frac{1}{4\pi}\frac{Re\{\gamma\}}{\lvert Im\{\gamma\}\rvert}$	4.9	0.69	0.43

material because it is CMOS compatible and less sensitive to temperature variations than organic materials.

7. Conclusions

We report nonlinear characterization of the real and imaginary parts of γ of a-Si samples, and a comparison with SOI waveguides. The measured FOM is 4.9, which is more than 7 times higher than for the SOI samples. On the other hand, time-resolved experiments did not show any slow response associated with carriers. This material has the additional advantage that it can be grown at the back-end of CMOS line, unlike SOI. These features make a-Si a suitable candidate for nonlinear all-optical switching applications.

Acknowledgments

We acknowledge financial support from the Spanish Ministry of Science and Innovation SINADEC (TEC2008-06333) and PROMETEO/2010/087 NANOFOTONICA projects and Universidad Politécnica de Valencia for PAID2011/1914 and J. Matres' doctoral grant.